

# Electrical manipulation of magnetic anisotropy in a $\text{Fe}_{81}\text{Ga}_{19}/\text{PMN-PZT}$ magnetoelectric multiferroic composite

W. Jahjah,<sup>1,2</sup> J.-Ph. Jay,<sup>1,\*</sup> Y. Le Grand,<sup>1</sup> A. Fessant,<sup>1</sup> A.R.E. Prinsloo,<sup>2</sup> C.J. Sheppard,<sup>2</sup> D.T. Dekadjevi,<sup>1,2</sup> and D. Spenato<sup>1</sup>

<sup>1</sup>Univ. Brest, Laboratoire d'Optique et de Magnétisme (OPTIMAG), EA 938, 29200 Brest, France

<sup>2</sup>Cr Research Group, Department of Physics, University of Johannesburg, PO Box 524, Auckland Park 2006, South Africa

(Dated: March 4, 2022)

Magnetoelectric composites are an important class of multiferroic materials that pave the way towards a new generation of multifunctional devices directly integrable in data storage technology and spintronics. This study focuses on strain-mediated electrical manipulation of magnetization in an extrinsic multiferroic. The composite includes 5 nm or 60 nm  $\text{Fe}_{81}\text{Ga}_{19}$  thin films coupled to a piezoelectric (011)-PMN-PZT. The magnetization reversal study reveals a converse magnetoelectric coefficient  $\alpha_{\text{CME,max}} \approx 2.7 \times 10^{-6} \text{ s.m}^{-1}$  at room temperature. This reported value of  $\alpha_{\text{CME}}$  is among the highest so far compared to previous reports of single-phase multiferroics as well as composites. An angular dependency of  $\alpha_{\text{CME}}$  is also shown for the first time, arising from the intrinsic magnetic anisotropy of FeGa. The highly efficient magnetoelectric composite FeGa/PMN-PZT demonstrates drastic modifications of the in-plane magnetic anisotropy, with an almost  $90^\circ$  rotation of the preferential anisotropy axis in the thinner films under an electric field  $E = 10.8 \text{ kV.cm}^{-1}$ . Also, the influence of thermal strain on the bilayer's magnetic coercivity is compared to that of a reference bilayer FeGa/Glass at cryogenic temperatures. A different evolution is observed as a function of temperature, revealing a substrate thermo-mechanical influence which has not yet been reported in FeGa thin films coupled to a piezoelectric material.

## I. INTRODUCTION

The research on the magnetoelectric (ME) coupling saw a renaissance [1] considering multiferroic (MF) materials in 2005 [2]. MF materials [3] simultaneously show at least two ferroic orderings, such as ferroelectric (FE) and (anti-)ferromagnetic as well as ferroelastic. There have recently been a frenzy over MF materials in condensed matter physics due to their novel potential applications, including multifunctional devices such as spintronics, ME transducers, actuators, sensors, and multiple-state memories [4–7]. Among multiferroic orderings, the coexistence of ferroelectricity and ferromagnetism is highly desired, as it allows electric-field control of magnetism without the need for magnetic fields, known as the converse ME effect (CME); the direct ME (DME) effect being the magnetic-field control of electric polarization [8]. Multiferroics may thus pave the way to faster, smaller, more energy-efficient data-storage technologies. The CME effect has been observed as an intrinsic effect in some oxide single-phase MF materials [9, 10] such as  $\text{BiFeO}_3$  (BFO), one of the few rare multiferroics at room temperature, thus the most intensively investigated single-phase multiferroics [11–14].

However, most of the single-phase MF materials possess either low permittivity or low permeability at room temperature and thus exhibit weak ME coupling which hinders their applications [15]. In addition, these materials are often complicated to fabricate, potentially lead-

ing to electrical leakage problems due to structural defects and impurities [14, 16]. ME composites, on the other hand, also known as extrinsic multiferroics, consist of stacked magnetostrictive and piezoelectric phases and offer a wide range of materials, as well as a flexibility in fabrication [17, 18]. These composites are a powerful tool to achieve, at room temperature, giant ME coupling response compared to those found in single-phase materials. Much efforts have been made to electrically control the magnetization via three main mechanisms: charge carrier [19–21], spin exchange (exchange bias coupling) [22–24], and strain-mediated coupling [20, 25–32]. Particularly, the strain-mediated mechanism has been found very appealing for further exploration [16, 33]. In strain-mediated composites, the ME coupling occurs when, in the case of CME, an applied electric field induces strain in the piezoelectric phase through the direct piezoelectric effect. This strain is transferred to the magnetostrictive phase and in turn induces inverse magnetostriction (Villari effect [34]), which translates to a change in magnetic properties.

In providing the strain, relaxor- $\text{PbTiO}_3$  (relaxor-PT) based ferroelectrics are widely used for their excellent piezoelectric properties. Rhombohedral  $\text{Pb}(\text{Mg}_{1/3}\text{Nb}_{2/3})\text{O}_3\text{-Pb}(\text{Zr,Ti})\text{O}_3$  (PMN-PZT) single crystals are an example of ternary-system ferroelectrics that provide, near their morphotropic phase boundary (MPB), many advantages when compared to their binary counterparts PMN-PT ( $\text{Pb}(\text{Mg}_{1/3}\text{Nb}_{2/3})\text{O}_3\text{-Pb}(\text{Ti})\text{O}_3$ ) and PZT-PT or PZT ceramics [35, 36]. They offer comparable piezoelectric coefficients ( $d_{33} = 1000 - 2000 \text{ pC.N}^{-1}$ ) and electromechanical coupling factors ( $k_{33} \geq 0.9$ ) compared to binary crystals, while possessing

\* jay@univ-brest.fr

double the coercive field values on the order of  $E_c = 5$  kV.cm<sup>-1</sup>, higher Curie temperature ( $T_c = 130 - 170^\circ$  C) and higher FE transition temperature ( $T_{RT} = 90 - 160^\circ$  C), significantly expanding the temperature range of usage for high-power applications [36, 37]. The piezoelectric coefficient notation  $d_{ij}$  refers to ‘ $j$ ’ axis as the working deformation direction under an applied  $E$  field along the polarization ‘ $i$ ’ axis, in compliance with the IEEE standards for relaxor-based FE single crystals [38].

Furthermore, it is possible to increase the strain amplitude by cutting and poling the crystal along particular crystallographic directions [39–42]. When the relaxor-PT crystals operate in the  $\langle 110 \rangle$ -poled longitudinal-transverse (L-T) mode (32 mode, vibration along  $\langle 001 \rangle$ ), they possess very high  $d_{32}$  and  $k_{32}$  values. Meanwhile, as the crystals are poled and driven through the thickness rather than the length, the required electric field to drive them is much lower than that for the L-L 33 mode [38, 43]. Consequently, a large in-plane anisotropic piezostress could be achieved, with  $d_{32} = -1850$  pC.N<sup>-1</sup> and  $d_{31} = 599$  pC.N<sup>-1</sup> in the (011)-PMN-PZT case [44–48]. This is a crucial driving mechanism to the observation of large anisotropic ME properties in combination with a magnetostrictive film.

Little focus has been given to such ternary relaxor ferroelectrics in electrically controlling the magnetism. In particular, (011)-PMN-PZT single crystals have only recently been used in controlling magnetization through CME coupling in ME composites [49], whereas they have shown a wide range of fresh interesting results in power generation and energy harvesting based on the DME effect [39, 41, 44–46, 48, 50–52]. Some of these works [39, 51] also involved galferol or FeGa as the magnetostrictive phase considering its promising magnetic properties.

Regarding the magnetostrictive phase, FeGa thin films combine remarkable properties such as low hysteresis, large magnetostriction, good tensile strength, machinability and recent progress in commercially viable methods of processing [53–55]. Although FeGa magnetostrictive properties are comparatively lower than those of Terfenol-D (a terbium-iron-dysprosium alloy), gallium, when substituted for iron increases the tetragonal magnetostriction coefficient  $\lambda_{100}$  over tenfold [53]. Another advantage of FeGa alloys is the rare-earth free composition; the cost is thus reduced compared to the rare-earth alloys family that also has another drawback which is brittleness.

FeGa has been the choice of magnetostrictive material for many studies, suggesting versatile proposals for the development of multifunctional devices exploiting both DME [56–58] and CME effects [9, 19, 24, 59–66]. Among these studies some have reported the dynamic self-biased effect, also called remanent CME, which is a desirable property recently sought to control the magnetization using an electric field in ME devices without the need for the assistance of an external biasing magnetic field [31, 49, 67–71]. Self-biased CME is indeed important

for lower-energy consumption and more compact ME devices.

Nevertheless, the CME coupling has not yet been investigated in a ME composite that brings together two highly performant components in the ME extrinsic multiferroics research such as the (011)-PMN-PZT ferroelectric single crystals and the magnetostrictive polycrystalline Fe<sub>81</sub>Ga<sub>19</sub> thin films.

Furthermore, the field of multiferroics covers aspects ranging from technological applications to fundamental research problems. The study of multiferroics increasingly influences neighbouring research areas, such as complex magnetism and ferroelectricity, oxide heterostructures and interfaces, etc [72]. This lead us to shed light over the bonding relationship of both phases in the extrinsic MF, and show how a different type of strain such as thermal strain at low temperatures can act on a magnetostrictive material depending on the substrate’s nature. This indeed has never been done before on the FeGa/PMN-PZT system.

In this contribution, we report on the magnetoelectric coupling in a Fe<sub>81</sub>Ga<sub>19</sub>/(011)-PMN-PZT composite through a systematic experimental study. For FeGa sample thicknesses  $t_{FM} = 5$  and 60 nm, magnetization reversal loops  $M(\mu_0 H)$  ( $\mu_0$  being the vacuum permeability) are first presented along the [100] and [011] directions and for only two electric field  $E$  values in section A. These measurements are then extended to bipolar  $E$ -field cycles to show the evolution of magnetic properties in section B. For more insight on anisotropy properties, we also present in section C the azimuthal behaviors of FeGa through angular measurements of  $M(\mu_0 H)$  under  $E = 0$  kV.cm<sup>-1</sup> and  $E > 0$  kV.cm<sup>-1</sup>. To quantify the relative magnetization change upon applying an electric field on our ME composite, we report in section D a CME coupling coefficient  $\alpha_{CME} = \mu_0 \Delta M / \Delta E$  (in s.m<sup>-1</sup>) among the highest reported so far, and compare it to a comprehensive literature recap of reported  $\alpha_{CME}$  values. We show as well an angular dependency of the  $\alpha_{CME}$  that is strongly related to the anisotropy properties of FeGa. In the final section E, low-temperature measurements ranging from 10 K to 300 K were carried out, in order to explore the thermo-magneto-mechanical effects by comparing the FeGa temperature-dependent magnetic coercivity’s behavior on two different substrates: amorphous glass and the single-crystalline ferroelectric PMN-PZT.

## II. EXPERIMENTAL PROCEDURES

Samples consisting of bi-layered ME composites are prepared by depositing the magnetostrictive FeGa thin films onto the piezoelectric (011)-PMN-PZT, using radio frequency (RF) magnetron sputtering. SSCG-grown (Solid State Crystal Growth) PMN-PZT rhombohedral single crystals are commercially available as *CPSC160-95* from Ceracomp Co. Ltd., Korea [73] The PMN-

PZT slabs are (011)-oriented and poled along the thickness, thus, along [011], creating an in-plane anisotropic strain behavior which allows the L-T working mode. This means that the (011) plane undergoes an anisotropic deformation while applying an electric field parallel to the [011] poling direction. Figure 1 presents the (011)-PMN-PZT unit cell along with the corresponding working mode.

As presented in Fig.1b, poling the crystal along the non-polar direction [011] creates a macro-symmetric multi-domain structure [39, 74] Such an engineered domain state is more stable than the single-domain state and offers an almost hysteresis-free strain- $E$  behavior, because the two dipole orientations  $\bar{[111]}$  and  $[111]$  are energetically equivalent and are equally populated under the [011] poling. When the (011)-oriented crystal is actuated by  $E$  parallel to [011], the two possible polar directions are expected to incline close to the  $E$  direction in each domain, which results in an increased rhombohedral lattice distortion and a large piezoelectric response. Such a move strongly deforms the (011) plane (marked in dashed blue lines): it induces simultaneously a strong compressive strain along the [100] direction ( $d_{32}$ ) and a tensile strain along the  $[0\bar{1}1]$  direction ( $d_{31}$ ) [30] This results in different signs and magnitudes of the planar piezoelectric coefficients, i.e.  $d_{32} = -1850$  pC.N $^{-1}$  and  $d_{31} = 599$  pC.N $^{-1}$ . Therefore the (011)-oriented PMN-PZT single crystal displays large anisotropic piezoelectric properties, with  $|d_{32}| \approx 3d_{31}$ .

Initially the PMN-PZT beams with dimensions  $7^L \times 5^W \times 0.3^T$  mm $^3$  were cleaned with ethanol and acetone. A Fe $_{81}$ Ga $_{19}$  polycrystalline target with a diameter of 3 inches was used in a *Oerlikon Leybold Univex 350* sputtering system. The base pressure prior to the film deposition was typically  $10^{-7}$  mbar. Fe $_{81}$ Ga $_{19}$  thin films were deposited onto the PMN-PZT beams at room temperature using 100 W deposition power, and about 10 sccm Argon pressure. The FM FeGa thicknesses were  $t_{\text{FM}} = 5$  and 60 nm. The stack was capped *in situ* with a 10 nm-thick Ta layer to protect the FeGa layer against oxidation. The growth was carried out under an in-plane magnetic field  $\mu_0 H_{\text{dep}} \sim 30$  mT (300 Oe) along the beam length, i.e. [100] direction (Fig.1a), in order to favor a preferential magnetic anisotropy direction. Other samples of FeGa/Ta with  $t_{\text{FM}} = 5$  and 60 nm were also deposited on Glass substrates (Schott D 263 TM [75]) which serve as reference samples.

For the electrical study, metallic electrodes must be available on both sides of the bi-layered ME composite. The 10 nm-thick Ta layer serves as a top electrode. For the bottom electrode, the samples were turned over and a 200 nm-thick Cu layer was deposited onto the bottom surface of the PMN-PZT beam using a mask of slightly smaller dimensions ( $6.5^L \times 4.5^W$  mm $^2$ ) than the PMN-PZT beam to avoid any short-circuit contact along the lateral edges with the FeGa. The final layered structure for our samples is Ta(10 nm)/FeGa( $t_{\text{FM}}$ )/PMN-PZT(0.3 mm)/Cu(200 nm) as shown in Fig.1a.

Static magnetic measurements were performed to probe the magnetization reversal with a commercial *Evico* MOKE microscope (Magneto-Optical Kerr Effect) [76]. An additional set-up within the MOKE apparatus was conceived to enable the application of an electric field across the sample thickness, thus allowing to perform magnetic measurements under an applied static electric field (Fig 1a). The as-deposited samples Ta(10 nm)/FeGa( $t_{\text{FM}}$ )/PMN-PZT(0.3 mm)/Cu(200 nm) were held on a support inside the electromagnet. The support base contains a bottom electrode that contacts the bottom Cu layer; and the top Ta layer is in contact with a thin brass needle tip as the top electrode. Both electrodes are wired to a DC power supply (up to 300 V), and an ammeter together with a 10 M $\Omega$  protecting resistor were series-wound in the circuit to monitor the current during all the measurements.

Furthermore, the coercive field temperature dependency was obtained from  $M(\mu_0 H)$  measurement using a *Cryogenic* cryogen-free physical properties measurement platform with a vibrating sample magnetometer (VSM) inset [77]. The magnet was initially demagnetized after which the sample was cooled in zero applied magnetic field to the desired temperature. The  $M(\mu_0 H)$  was then measured using the low magnetic field option of the Cryogenic system.

### III. RESULTS AND DISCUSSION

#### A. Electrical tuning of the magnetization reversal

Electric-field control of magnetization was carried out using MOKE that supported an additional *in situ* set-up to enable the application of an electric field across the sample thickness. The  $E$  pointing from the PMN-PZT to the FeGa film was defined as the positive  $E$  (Fig.1). Routinely, the magnetization hysteresis loops were measured along the [100] direction ( $\varphi = 0^\circ$ ) and the  $[0\bar{1}1]$  direction ( $\varphi = 90^\circ$ ) under different values of applied electric field  $E$ : 0 kV.cm $^{-1}$ , 6.5 kV.cm $^{-1}$  and 10 kV.cm $^{-1}$ , as presented in Fig.2. We will characterize these loops using the quantities  $\mu_0 H_c$  as the coercive field, and  $M_r^n$  as the remanent magnetization normalized to the saturation magnetization, which is equivalent to the squareness (i.e.  $M_r^n = M_r/M_s$ ).

Under no applied  $E$ , the 5 nm-thick FeGa sample's  $M(\mu_0 H)$  loops show an angular dependency when comparing  $\mu_0 H_c$  and  $M_r^n$  for both presented angles  $\varphi = 0^\circ$  and  $90^\circ$ . As for the 60 nm-thick sample, the  $M(\mu_0 H)$  loops show a much less significant angular dependency;  $\mu_0 H_c$  and  $M_r^n$  show very close values for both angles. The measured values of  $\mu_0 H_c$  and  $M_r^n$  are typical of those observed for FeGa thin films [55].

For both  $t_{\text{FM}} = 5$  and 60 nm,  $\mu_0 H_c$  and  $M_r^n$  values along [100] decrease when  $E$  increases, making the cycles more slanted than square. An easy magnetic anisotropy

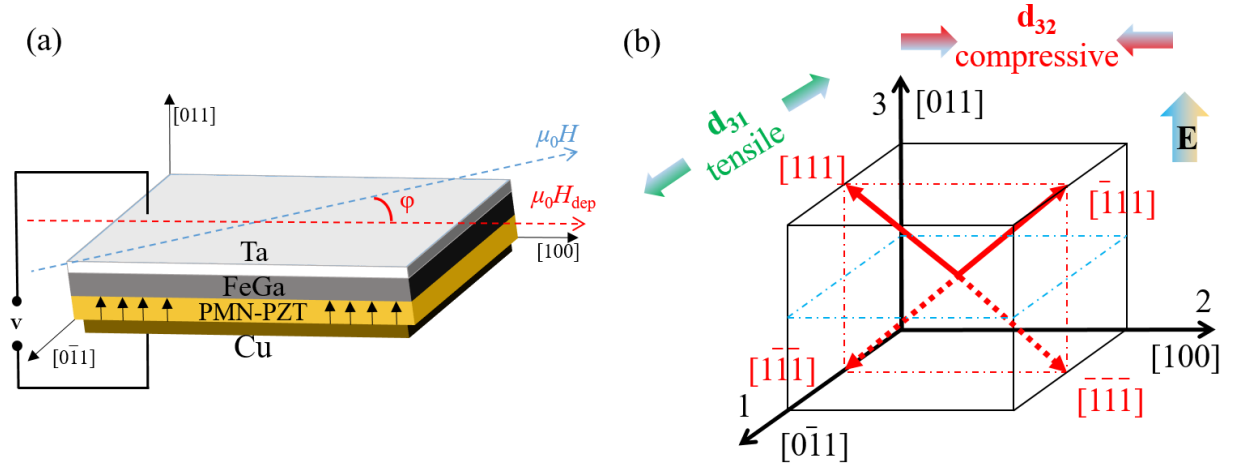


FIG. 1. (a) Schematic drawing of the ME composite consisting of the magnetostrictive FeGa and the (011)-oriented PMN-PZT beam. The configuration of measurement is also indicated using  $\varphi$  angle between the applied magnetic field  $\mu_0 H$  (dashed blue axis) and the deposition field  $\mu_0 H_{\text{dep}}$  (dashed red axis along the [100] length of the beam). Black arrows inside the PMN-PZT layer represent the positive electric field direction. Drawing is not to scale. (b) Sketch of the polarization vectors of the rhombohedral PMN-PZT unit cell in the (011)-oriented case. Also presented are the  $d_{31}$  and  $d_{32}$  modes of strain, the electric field  $E$  poling direction along [011] with its plane (dashed blue square).

axis along [100] clearly becomes a harder axis under the application of  $E$ . The situation changes when looking at the  $[0\bar{1}1]$  direction, where  $\mu_0 H_c$  and  $M_r^n$  values increase when  $E$  increases, and the cycles become more square than slanted. In this case a hard anisotropy axis along  $[0\bar{1}1]$ , especially for the 5 nm-thick sample, becomes an easier axis. These converse reversal behaviors are tightly related to the (011)-PMN-PZT anisotropic strain induced by  $E$ : simultaneously a strong in-plane compressive strain along [100] ( $d_{32}$ ) weakens the anisotropy's easy character and a tensile strain along  $[0\bar{1}1]$  ( $d_{31}$ ) weakens its hard character.

The  $E$ -field dependency of  $M(\mu_0 H)$  loops along [100] and  $[0\bar{1}1]$ , thus, suggests a first sign of a switching of a magnetic anisotropy easy axis. Such an axis, when aligned along  $\mu_0 H_{\text{dep}}$ , will tend to align under  $E$  in the direction of tensile stress for positive magnetostriction  $\lambda$ , i.e. the  $[0\bar{1}1]$  direction. Hence, the total energy is minimized, including the magnetoelastic term  $E_{\text{me}} = -(3/2)\lambda\sigma \cos^2 \theta$  [34], where  $\sigma$  is the applied stress and  $\theta$  the angle between magnetization and stress.

In Section C we will provide azimuthal measurement in order to provide more insight into the anisotropy behaviour of the samples.

## B. Bipolar $E$ -field measurements

The strain-mediated electric control of magnetization can be extended to a bipolar measurement cycle in which the electric field is swept through positive and negative values. We have performed such cycling as follows:  $E = +10.8 \text{ kV.cm}^{-1} \rightarrow 0 \text{ kV.cm}^{-1} \rightarrow -10.8 \text{ kV.cm}^{-1} \rightarrow 0 \text{ kV.cm}^{-1}$  and finally back to the initial  $+10.8 \text{ kV.cm}^{-1}$ , with a  $1.6 \text{ kV.cm}^{-1}$  step. In the strain-mediated FM/FE

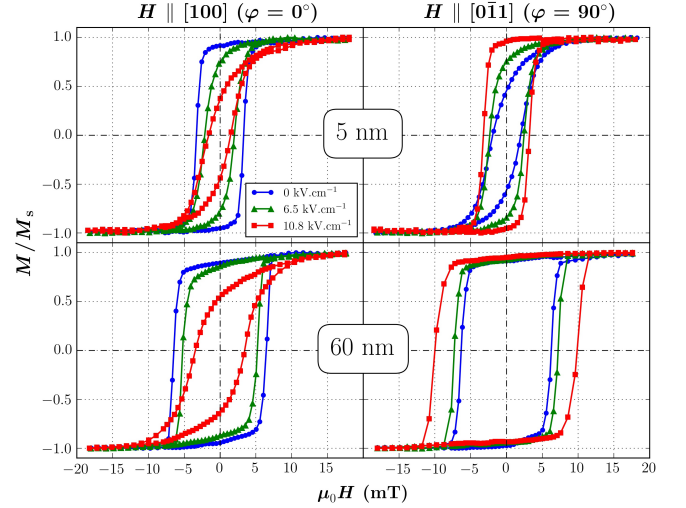


FIG. 2. Hysteresis loops of the normalized magnetization reversal of the Ta(10 nm)/FeGa( $t_{\text{FM}} = 5; 60 \text{ nm}$ )/PMN-PZT(0.3 mm)/Cu(200 nm), measured in-plane with the magnetic field  $\mu_0 H$  respectively parallel to [100] ( $\varphi = 0^\circ$ , i.e. along the deposition field axis  $\mu_0 H_{\text{dep}}$ ) and  $[0\bar{1}1]$  ( $\varphi = 90^\circ$ , under three values of electric field  $E = 0, 6.5$  and  $10.8 \text{ kV.cm}^{-1}$ .

two-phase system, the bipolar- $E$ -field controlled magnetization generally exhibits a butterfly-shaped behavior and the understanding of it has been well established in terms of the piezostain of the FE substrate transferred to the FM layer [29, 78–81].

In CME reports, it is common to probe the bipolar- $E$ -field tuning of the magnetic moment as  $M(E)$  loops, under a constant static magnetic bias field  $\mu_0 H$  and quantify the relative change of  $M$  [26, 28, 30, 79, 82, 83]. Another way of probing the electrically-induced change

in magnetization would be extracting  $M_r^n$  from  $M(\mu_0 H)$  as function of  $E$  loops [84], as the ones in Fig.2. In the following, we will quantify the relative change of  $M_r^n$  extracted from  $M(\mu_0 H)$  loops under incremented  $E$  values as:  $\Delta M_r^n / M_r^n(0) = (M_r^n(E_{\max}) - M_r^n(0)) / M_r^n(0)$ .

We can see in Fig.3 the nonlinear cycles representing the evolution of  $\mu_0 H_c$  and  $M_r^n$  as a function of  $E$  along both [100] and  $[0\bar{1}1]$  directions. As mentioned earlier in section II, the magnetic bipolar loops in Fig.3 agree well with a low-hysteresis behavior of the (011)-PMN-PZT piezostain, an almost reversible tuning of magnetization with positive and negative  $E$ , and most importantly a remarkable modification of the magnetic properties. For instance, by looking at the 5 nm-thick sample,  $M_r^n(E)$  along [100] undergoes a  $\Delta M_r^n / M_r^n(0) \approx 72\%$  relative decrease upon applying  $E_{\max} = 10.8 \text{ kV.cm}^{-1}$ . Such relative decrease of magnetization has been previously observed in  $\text{Co}_{40}\text{Fe}_{40}\text{B}_{20}(20\text{nm})/(\text{011})\text{-PMN-PT}$  [30] and in  $\text{FeAl}(10 \text{ nm})/\text{PIN-PMN-PT}$  [82]

In the case of the 60 nm-thick sample,  $\Delta M_r^n / M_r^n(0)$  is reduced to  $\approx 33\%$ . This decrease with thickness can be associated with the reduced magnetoelastic coefficient in FeGa films with increasing thickness, as we have shown in our previous study [55]. Although the (011)-PMN-PZT piezostain is strong enough to influence the thin FeGa films, and the direct bonding of the two materials (using the sputtering technique) is among the best techniques for maximum strain transfer, the magnetostriction of the FM phase is an important factor that drives the strain-mediated control of magnetization.

The relative change  $\Delta M_r^n / M_r^n(0)$  along  $[0\bar{1}1]$  follows the opposite trend.  $M_r^n(E)$  increases by  $\Delta M_r^n / M_r^n(0) \approx 80\%$  when  $E = 10.8 \text{ kV.cm}^{-1}$  is applied for the 5 nm-thick sample.  $M_r^n(E)$  is practically unchanged for the 60 nm-thick sample, which is in agreement with the  $M(\mu_0 H)$  results in Fig.2.

We also note that the electric fields corresponding to the maximum (respectively minimum)  $M_r^n(E)$  along [100] (respectively  $[0\bar{1}1]$ ) in Fig.3 are  $\approx \pm 2 \text{ kV.cm}^{-1}$ , which is smaller than the coercive field of PMN-PZT  $E_c = 4 \text{ kV.cm}^{-1}$ . This has been previously observed in similar ME composites [26]. In an ideal case, a ferroelectric  $P - E$  or  $S - E$  loop is symmetrical, so the positive and negative  $E_c$  are equal and correspond to FE domains switching. Experimentally, the  $E_c$  value is not an absolute threshold for FE domains switching, which may start for  $E$  values smaller than  $E_c$ . These FE properties may be affected by many factors that shape a ferroelectric  $P - E$  or  $S - E$  loop including the thickness of the sample, presence of charged defects, mechanical stresses, preparation conditions, thermal treatment [85], and relaxation effects of switching FE domains [30].

In addition, Fig.3 shows an asymmetry of the  $M_r^n(E)$  and  $\mu_0 H_c(E)$  curves by looking at the highest  $E = \pm 10.8 \text{ kV.cm}^{-1}$ , most noticeably the  $M_r^n(E)$  curves along [100]. This asymmetry may arise from the aforementioned factors, and has been observed previously in magnetoelectric composites [20, 26, 28, 82–84]. Small rema-

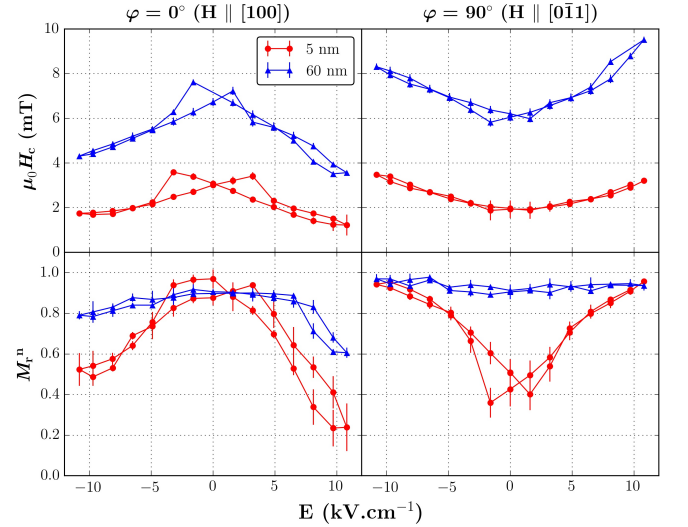


FIG. 3. Electric-field control of the coercive field  $\mu_0 H_c$  (top row) and the remanent magnetization normalized to the saturation magnetization  $M_r^n$  (bottom row) along both directions [100] (left column) and  $[0\bar{1}1]$  (right column) for the Ta(10 nm)/FeGa( $t_{\text{FM}} = 5$ ; 60 nm)/PMN-PZT(0.3 mm)/Cu(200 nm) samples. The lines are guides to the eyes.

nent strain states may be responsible for such asymmetry [84]. It is also presumed that an internal field in the PMN-PZT may be generated, originating from different kinds of defects (e.g. structure, fatigue, relaxation) in the FE substrate [29, 81, 86–90].

### C. Magnetic azimuthal evolutions under $E$

The previous electric-field control of magnetization results have so far been presented for the two characteristic directions [100] ( $\varphi = 0^\circ$ ) and  $[0\bar{1}1]$  ( $\varphi = 90^\circ$ ) of the (011)-PMN-PZT. Indeed depending on thickness, FeGa exhibits a considerable angular dependency of magnetic properties as shown in Fig.2. It would be of interest to study this azimuthal dependency to further understand the anisotropy configuration by rotating the sample in its plane by the angle  $\varphi$  with respect to  $\mu_0 H_{\text{dep}}$ . In-plane magnetization reversal measurements were performed each 10 degrees. The azimuthal evolutions of  $\mu_0 H_c$  and  $M_r^n$  as a function of  $E$  are reported for all samples in Fig.4.

Under  $E = 0 \text{ kV.cm}^{-1}$ , the 5 nm-thick sample shows two maxima of  $\mu_0 H_c$  and  $M_r^n$  lying along [100] or  $\varphi = 0^\circ$ . The axis carrying these maxima will be referred to as the “maxima axis”, and in this case lies along the  $\mu_0 H_{\text{dep}}$  direction. Two smaller local maxima of  $\mu_0 H_c$  also appear at  $\varphi = 90^\circ$ . The angular dependency of  $\mu_0 H_c$  indicates a cubic component of the magnetic anisotropy. This has been already observed in our previous work which revealed a magnetic anisotropy with a predominant in-plane cubic component in thin FeGa films (5 nm) deposited onto glass substrate [55].

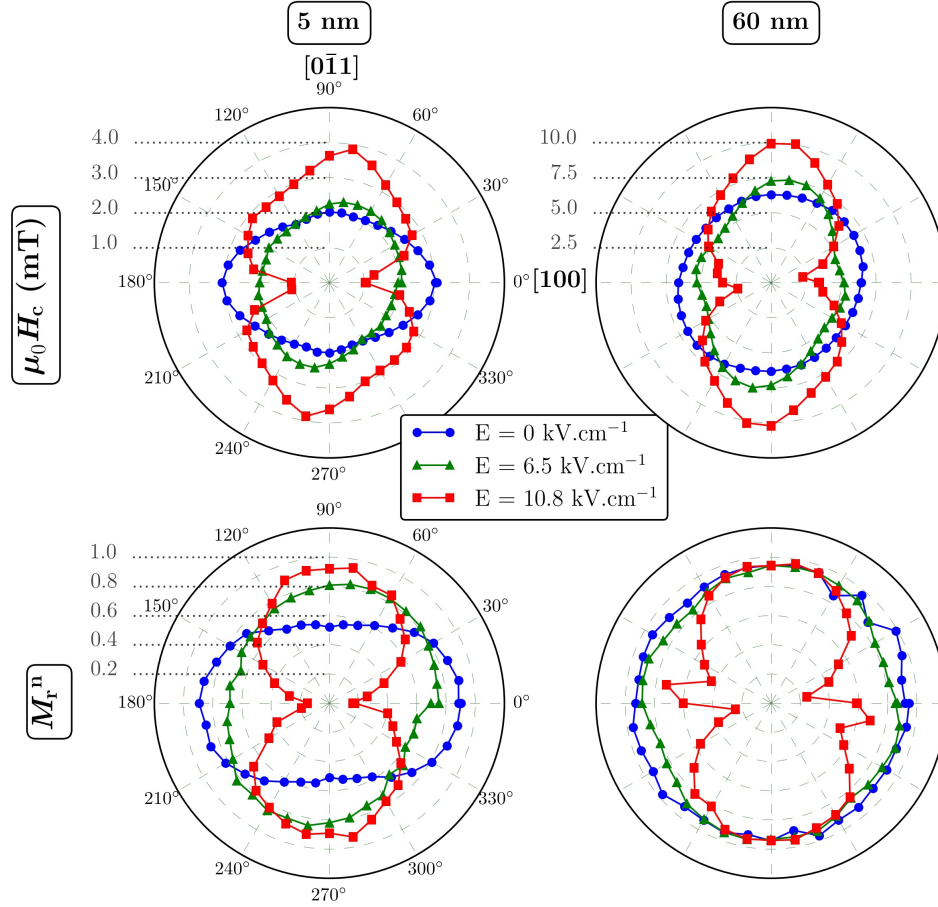


FIG. 4. Azimuthal evolutions of the coercive field  $\mu_0 H_c$  (first row) and the remanent magnetization normalized to the saturation magnetization  $M_r^n$  (second row) extracted from  $M(\mu_0 H) - \varphi$  loops. The external magnetic field  $\mu_0 H$  is applied at the varying angle  $\varphi$  on the Ta(10 nm)/FeGa( $t_{\text{FM}} = 5; 60$  nm)/PMN-PZT(0.3 nm)/Cu(200 nm) samples and under the three considered values of electric field  $E = 0, 6.5$  and  $10.8$  kV.cm $^{-1}$ .  $\mu_0 H_{\text{dep}}$  is applied along [100] ( $\varphi = 0^\circ$ ).

Applying an electric field  $E = 6.5$  kV.cm $^{-1}$  rotates the maxima axis by almost  $70^\circ$ , and a stronger field  $E = 10.8$  kV.cm $^{-1}$  rotates it further towards the  $[0\bar{1}1]$  direction by  $80^\circ$ . Indeed applying  $E = 10.8$  kV.cm $^{-1}$  also changes the azimuthal shape of  $\mu_0 H_c$  and  $M_r^n$  which is typical of a uniaxial anisotropy (i.e. two  $\mu_0 H_c$  maxima at  $\varphi = 80^\circ$ , two  $M_r^n$  maxima at  $\varphi = 90^\circ$ , and two minima at  $\varphi = 0^\circ$ ). This amount of maxima axis rotation is higher than the reported  $55^\circ$  value in FeAl(10 nm)/PIN-PMN-PT under  $E = 10 - 12$  kV.cm $^{-1}$  [82]. It is worth noting that the  $\mu_0 H_c$  maxima have higher values  $\mu_0 H_{c,\text{max}} = 4$  mT under the highest  $E = 10.8$  kV.cm $^{-1}$  compared to the maxima  $\mu_0 H_{c,\text{max}} = 3$  mT under no applied  $E$ . The same remark can be done for the 60 nm-thick sample [30].

Under no applied  $E$ , the situation is different for the 60 nm-thick sample: the angular dependency of  $\mu_0 H_c$  is quasi-circular, revealing a random magnetic anisotropy dispersion [91, 92]. This has also been observed in our previous paper [55], in which the cubic component of the 5 nm-thick films faded away, but did not vanish, to a more random anisotropy dispersion with increasing thicknesses ( $\geq 20$  nm). Such behavior was attributed to a predomi-

nant texture in thinner films which, in thicker films, is replaced by a non-preferential polycrystalline arrangement. Cullen et al. [91] suggests that a competition between coherent and randomly oriented local anisotropies leads to zero or very small net anisotropy in FeGa thin films with almost the same composition ( $\sim 20\%$  Ga content). In a recent study [92], magnetic domain structure observations in FeGa/MgO thin films evidenced this competition between the coherent cubic anisotropy and the random anisotropy contribution.

Under the highest field  $E = 10.8$  kV.cm $^{-1}$ , two maxima of  $\mu_0 H_c$  and  $M_r^n$  appear at  $\varphi = 80^\circ$  and are accompanied by the development of two local maxima of  $M_r^n$  close to  $\varphi \sim 0^\circ$ . It is clear that the random anisotropy character vanishes, leaving out a coexistence of the coherent cubic and uniaxial components under the strain. Under the field  $E = 6.5$  kV.cm $^{-1}$ , an intermediate behavior is observed.

#### D. Magnetoelectric coefficient $\alpha_{\text{CME}}$

To quantify the electric-field-induced variation of magnetic properties, it is convenient to introduce the converse magnetoelectric coupling coefficient defined by  $\alpha_{\text{CME}}$  (expressed in  $\text{s.m}^{-1}$ ), which represents the variation of the magnetization under an applied electric field.

Several methods may be used to calculate  $\alpha_{\text{CME}}$ . The first one (method *a*) is to consider  $\alpha_{\text{CME}}$  as the slope (first derivative) of a  $M(E)$  loop, i.e. directly measuring the magnetization change as a function of a changing electric field either under a constant static magnetic bias field  $\mu_0 H$  [8, 25, 26, 30, 49, 82, 93], or by saturating the FM film with  $\mu_0 H$  and then removing it [83]. In another method (method *b*),  $\alpha_{\text{CME}}$  is determined by computing the magnetization from magnetoresistance loops measurements in a spin-valve device [94]. In our case, an alternative method (method *c*) consists of calculating  $\alpha_{\text{CME}}$  using the following equation [27, 28]:

$$\begin{aligned}\alpha_{\text{CME}}(\mu_0 H) &= \mu_0 \frac{\Delta M_{E_0}(\mu_0 H)}{\Delta E} \\ &= \mu_0 \frac{M_{E=E_0}(\mu_0 H) - M_{E=0}(\mu_0 H)}{E_0},\end{aligned}$$

with  $E_0 = 6.5$  or  $10.8 \text{ kV.cm}^{-1}$ . This relative change in magnetization under an applied electric field  $E$  is directly computed from the  $M(\mu_0 H)$  loops presented in Fig.2.

The FeGa thin films in this study have a saturation magnetization  $\mu_0 M_s = 1.15 \text{ T}$  [55]; we can thus deduce the  $\alpha_{\text{CME}}$  values in  $\text{s.m}^{-1}$  as shown in Fig.5 along both characteristic directions [100] and  $[0\bar{1}1]$  of the (011)-PMN-PZT.

The results reveal a maximum  $\alpha_{\text{CME}} = 2.4 \times 10^{-6} \text{ s.m}^{-1}$  for the 60 nm-thick sample along [100]. This value is indeed obtained for lower  $\Delta E = 6.5 \text{ kV.cm}^{-1}$ , and for magnetic bias field values near  $\mu_0 H_c$ . Also, for the 5 nm-thick sample, a higher  $\alpha_{\text{CME}} = 1.5 \times 10^{-6} \text{ s.m}^{-1}$  is obtained along [100] than along  $[0\bar{1}1]$ . Indeed, these results are correlated with the fact that the magnetization reversal loops in Fig.2 are more significantly modified along [100] than along  $[0\bar{1}1]$  under  $E = 6.5 \text{ kV.cm}^{-1}$ .

Besides, it is interesting to see non-zero  $\alpha_{\text{CME}}$  values at zero bias field  $\mu_0 H = 0$ , especially for the 5 nm-thick sample:  $\alpha_{\text{CME}} \sim 0.7 \times 10^{-6} \text{ s.m}^{-1}$  for  $H//[100]$  and  $\Delta E = 10.8 \text{ kV.cm}^{-1}$ . These values correspond to a remanent magnetoelectric coupling at zero bias field  $\mu_0 H$ , which is related to the hysteretic magnetic behavior and the strong remanent magnetization [49, 71]. This is truly encouraging for the dynamic CME self-biased potential of FeGa/PMN-PZT in applications, which is revealed in measurements that assess the magnetization change under an alternating AC electric field superimposed to a DC magnetic bias field  $\mu_0 H$  (yielding a non-zero remanent CME( $\mu_0 H$ ) at  $\mu_0 H = 0$ ) [31, 67–69].

Furthermore, as we have performed azimuthal measurements shown in Fig.4 to assess the angular dependencies of  $\mu_0 H_c$  and  $M_r^n$ , this led us to believe that the

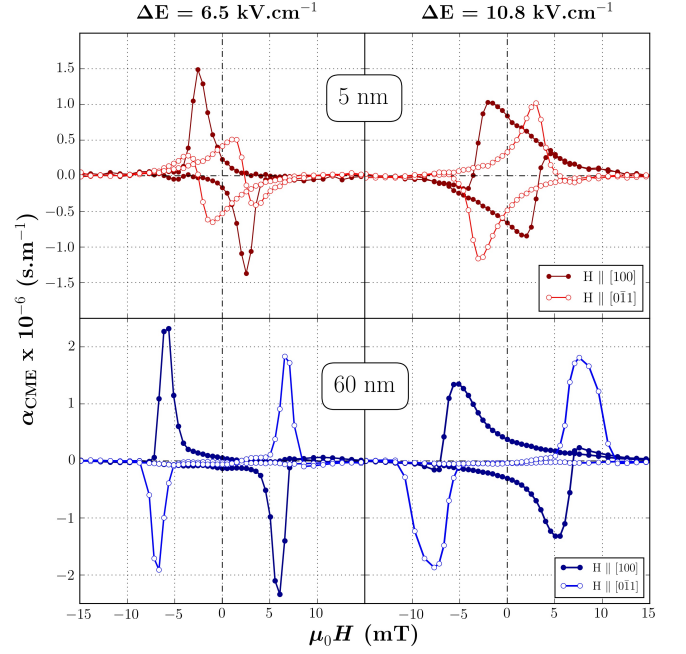


FIG. 5. The converse magnetoelectric coupling coefficient  $\alpha_{\text{CME}}$  as calculated from  $M(\mu_0 H)$  data in Fig.2 for the Ta(10 nm)/FeGa( $t_{\text{FM}} = 5$ ; 60 nm)/PMN-PZT(0.3 nm)/Cu(200 nm) samples, under  $\Delta E = 6.5$  and  $10.8 \text{ kV.cm}^{-1}$ .

CME behavior may rely specifically on certain non trivial orientations  $\varphi$  rather than only the crystallographic [100] and  $[0\bar{1}1]$  directions. We have, thus, calculated the angular dependency of  $\alpha_{\text{CME}}$  by applying the same method used in Fig.5 to the  $M(\mu_0 H) - \varphi$  loops used in Fig.4. The maximum value of  $\alpha_{\text{CME}}$  is subsequently plotted as  $\alpha_{\text{CME,max}}$  for each angle  $\varphi$  in Fig.6.

The angular behavior of  $\alpha_{\text{CME,max}}$  shows peculiar symmetry shapes especially under  $\Delta E = 6.5 \text{ kV.cm}^{-1}$ . This confirms that the as-considered  $\alpha_{\text{CME}}$  method (*c*) depends exclusively on the measured  $M(\mu_0 H) - \varphi$  loops' characteristics related to both  $\mu_0 H_c$  and  $M_r^n$ . We remind the reader that these  $\alpha_{\text{CME,max}}$  correspond to peak values of  $\alpha_{\text{CME}}$  for bias field values  $\mu_0 H$  close to  $\mu_0 H_c$  (Fig.5), and not  $\alpha_{\text{CME}}$  taken at zero bias field  $\mu_0 H$ . The zero bias field  $\mu_0 H$  corresponds exclusively to the  $M_r^n(E)$  case that was explored in Fig.3.

By looking at the 60 nm-thick sample, we can deduce an even higher value than the ones obtained at  $\varphi = 0^\circ$  and  $90^\circ$  of  $\alpha_{\text{CME,max}} \approx 2.7 \times 10^{-6} \text{ s.m}^{-1}$  at  $\varphi = 30^\circ$ . Such results are reported for the first time and indeed confirm the anisotropic nature of CME in anisotropic FeGa thin films. A stronger electric field  $E = 10.8 \text{ kV.cm}^{-1}$  brings about a more uniform four-fold symmetry of the  $\alpha_{\text{CME,max}}$  for all samples. Two maxima values  $\alpha_{\text{CME,max}} \approx 1.8 \times 10^{-6} \text{ s.m}^{-1}$  are found around  $\varphi = 90^\circ$  and two lower maxima around  $\varphi = 0^\circ$ . This behavior is similar to the stronger  $\mu_0 H_c$  modification by  $E$  along  $[0\bar{1}1]$ .

To our knowledge, this value of  $\alpha_{\text{CME}}$  obtained at room temperature is several orders of magnitude higher than the reported values for single-phase multiferroics in the CME literature, as well as higher than or comparable to reported values in other composite multiferroics. In Table I a comprehensive list is given of the reported CME values.

It is important to note that such a high achievable  $\alpha_{\text{CME}}$  is obtained within a unipolar measurement of  $|\Delta E| = |0 - 6.5| \text{ kV.cm}^{-1}$  with a non-180° polarization switching of the (011)-PMN-PZT ferroelectric domains (as explored in the bipolar measurements in Fig.3), which is expected to fatigue the FE single crystal, induce relaxation effects, and alter the performance of ME devices [78, 87]. Therefore, electric-field control of magnetization in the unipolar case should be preferred for example for the high-speed applications of SME-RAMs (*Strain-mediated MagnetoElectric Random Access Memory*) in similar structures [5]. Another key point is that our value of  $\alpha_{\text{CME}}$  coupling is obtained in a static non-resonant mode of measurement. This is not only promising for realizing non-resonant ME devices, but also appealing to perform dynamic measurements which are expected to boost this value of  $\alpha_{\text{CME}}$ , but are beyond the scope of this study.

Thus, the tunable converse ME effect reported here is particularly significant in terms of strong magnetization reversal variation. Finally, even if a higher  $\alpha_{\text{CME}}$  is achieved with the thicker 60 nm FeGa film, it is noteworthy that  $\alpha_{\text{CME}}$  of the thinner 5 nm film is still high enough compared to the other reported values for thicker films in Table I. The 5 nm film offers also the advantage of a non-zero remanent  $\alpha_{\text{CME}}$ , i.e. at  $\mu_0 H = 0$ .

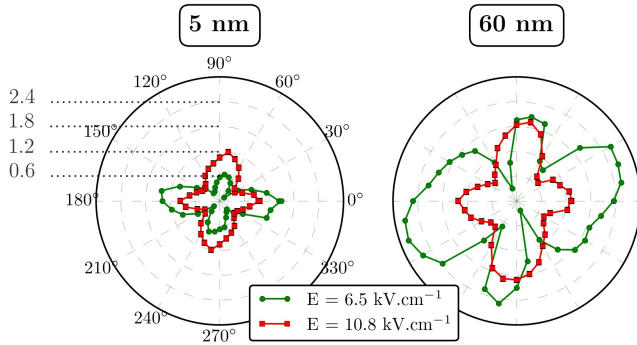


FIG. 6. Azimuthal evolution of the maximum of the converse magnetoelectric coupling coefficient  $\alpha_{\text{CME,max}}$  as calculated in Fig.5, and extracted from  $M(\mu_0 H) - \varphi$  azimuthal data of the Ta(10 nm)/FeGa( $t_{\text{FM}} = 5$ ; 60 nm)/PMN-PZT(0.3 mm)/Cu(200 nm), under  $\Delta E = 6.5$  and  $10.8 \text{ kV.cm}^{-1}$ .

### E. Thermo-mechanical effects

In the previous sections the magnetoelectric effect has been investigated in the FeGa/PMN-PZT compos-

Multiferroic system	$\alpha_{\text{CME}}$ (s.m <sup>-1</sup> )	T(K)	ref.
CoFe <sub>2</sub> O <sub>4</sub> (200 nm)/PMN-PT	$3.2 \times 10^{-8}$ *	300	[26]
La <sub>0.7</sub> Sr <sub>0.3</sub> MnO <sub>3</sub> (20–50nm)/PMN-PT	$6.0 \times 10^{-8}$ *	330	[25]
Co <sub>0.9</sub> Fe <sub>0.1</sub> (2.3nm)/Cu/Co <sub>0.9</sub> Fe <sub>0.1</sub> (2.5nm)/BiFeO <sub>3</sub>	$1.0 \times 10^{-7}$ **	300	[94]
La <sub>0.67</sub> Sr <sub>0.33</sub> MnO <sub>3</sub> (40nm)/BaTiO <sub>3</sub>	$2.3 \times 10^{-7}$ *	157	[8]
YIG(600nm)/PMN-PZT	$3.1 \times 10^{-7}$ *	300	[49]
La <sub>0.7</sub> Ca <sub>0.3</sub> MnO <sub>3</sub> (10 nm)/BaTiO <sub>3</sub>	$5 \times 10^{-7}$ ***	20	[27]
Terfenol-D/PZT	$7.8 \times 10^{-7}$	300	[95]
FeRh(22nm)/BaTiO <sub>3</sub>	$1.4 \times 10^{-6}$ *	385	[93]
Fe <sub>81</sub> Al <sub>19</sub> (10 nm)/PIN-PMN-PT	$1.6 \times 10^{-6}$ *	300	[82]
Co <sub>40</sub> Fe <sub>40</sub> B <sub>20</sub> (20nm)/PMN-PT	$2.0 \times 10^{-6}$ *	300	[30]
<b>Fe<sub>81</sub>Ga<sub>19</sub>(60nm)/PMN-PZT</b>	<b><math>2.7 \times 10^{-6}</math> ***</b>	<b>300</b>	<b>this work</b>
Fe <sub>50</sub> Co <sub>50</sub> (80nm)/Ag/PIN-PMN-PT	$3.5 \times 10^{-6}$ ***	300	[28]
Co <sub>40</sub> Fe <sub>40</sub> B <sub>20</sub> (50nm)/PMN-PT	$8.0 \times 10^{-6}$ *	300	[83]

TABLE I. Literature recap of converse magnetoelectric coupling coefficient  $\alpha_{\text{CME}}$  values (in s.m<sup>-1</sup>) for different magnetoelectric composite materials. \*: method *a* of  $\alpha_{\text{CME}}$  computing, \*\*: method *b* and \*\*\*: method *c*.

ite. The strain driven by an applied electric-field on the PMN-PZT substrate indeed manipulates the FeGa magnetization state and anisotropy.

Another parameter that may modify the internal strain and stress – and, thus, the magnetic anisotropy through inverse magnetostriction – is temperature through thermal expansion. Temperature is an important factor for the stability of ME devices operating in complex environments. ME effect has only rarely been reported at low temperatures for power generation (DME) [96, 97]. However measuring the temperature-dependent ME effect in our samples is beyond the scope of this study. Instead we have aimed to examine the potential influence of the PMN-PZT substrate’s thermal expansion on the FeGa magnetic properties as a function of temperature, in order to gain more insight on how thermal strain can act on a magnetostrictive material deposited on ferroelectric single crystals.

We have performed magnetic temperature measurements, using a *Cryogenic* free physical properties measurement platform with a VSM insert. The sample is zero-field cooled (ZFC) to the desired temperature (from 300 K down to 10 K as an example), then  $M(\mu_0 H)$  is measured, from which we can extract the coercive field  $\mu_0 H_c$ . We note that the results were the same in both ZFC and field-cooled (FC) modes. We used two different substrates for the purpose of discriminating between the FM thermal expansion and that of the substrate: amorphous glass and the single-crystalline ferroelectric PMN-PZT. Samples, thus, consist of Ta(10 nm)/FeGa( $t_{\text{FM}} = 5$ ; 60 nm)/PMN-PZT(0.3 mm) and the reference bilayer Ta(10 nm)/FeGa( $t_{\text{FM}} = 5$ ; 60 nm)/Glass(0.5 mm). The corresponding  $M(\mu_0 H)$  loops are presented in Fig.7 for both temperatures 300 K and 10 K.

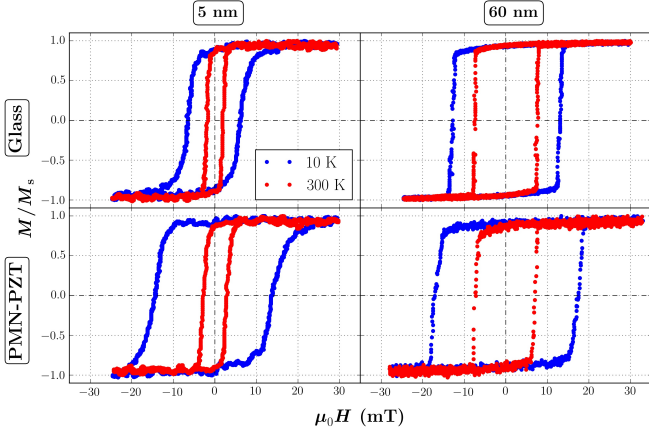


FIG. 7. Hysteresis loops of the normalized magnetization reversal at 300 K and 10 K of the Ta(10 nm)/FeGa( $t_{\text{FM}} = 5$ ; 60 nm)/PMN-PZT(0.3 mm) and FeGa( $t_{\text{FM}} = 5$ ; 60 nm)/Glass/Ta(10 nm), measured in-plane with the magnetic field  $\mu_0 H$  parallel to [100] ( $\varphi = 0^\circ$ , i.e. along the deposition field axis  $\mu_0 H_{\text{dep}}$ ).

$M(\mu_0 H)$  loops in Fig. 7 show a drastic influence of temperature on  $\mu_0 H_c$  values. The remanence however is not affected. For both thicknesses,  $\mu_0 H_c$  values are similar at room temperature 300 K on both substrates. At 10 K, these values diverge depending on the substrate.

The evolution of  $\mu_0 H_c$  as a function of the measuring temperature for both substrates and  $t_{\text{FM}}$  are presented in Fig. 8.  $\mu_0 H_c$  typically decreases with increasing temperature, as a result of thermal agitation [13, 55]. Nevertheless, comparing one  $t_{\text{FM}}$  of FeGa on both substrates (blue and orange circles) reveals a clear difference in the curve slope  $\Delta(\mu_0 H_c)/\Delta T$ . Therefore below 300 K,  $\mu_0 H_c$  values of one FeGa  $t_{\text{FM}}$  gradually diverge when comparing both substrates. In particular,  $\mu_0 H_c$  of the 5 nm-thick sample increases between 300 K and 10 K approximately sixfold on PMN-PZT, whereas on glass it increases threefold. It is also noteworthy that the  $\mu_0 H_c(T)$  curve slope  $\Delta(\mu_0 H_c)/\Delta T$  is independent of the film thickness, by revealing almost parallel curves (color-filled or open circles) of both  $t_{\text{FM}}$  on a single substrate. This has also been shown in Fig. 7 of our previous work [55].

A similar substrate-dependent trend of  $\mu_0 H_c$  evolution at low temperatures was also observed when comparing exchange biased FeGa/IrMn bilayers deposited onto piezoelectric PVDF for electrical manipulation, and on Si substrates [98].

Consequently, at low temperatures, when FeGa is grown on the piezoelectric PMN-PZT, its coercivity responds differently to thermal strain compared to the growth on glass. This indeed reveals a combined thermomagneto-mechanical effect, which has been previously observed in other systems [98–100]. Such phenomena may be attributed to the difference in the elastic properties of both glass and PMN-PZT substrates [40, 97].

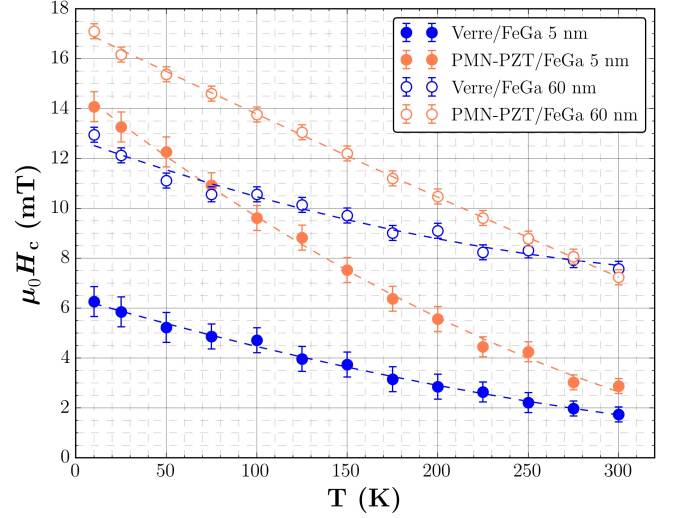


FIG. 8. Temperature-dependent evolution of the coercive field  $\mu_0 H_c$  of 5 and 60 nm-thick FeGa samples (respectively filled and empty circles) deposited onto two different substrates: Glass (blue circles) and (011)-PMN-PZT (orange circles). The dashed lines are guides to the eyes.

#### IV. CONCLUSION

In summary, we demonstrate an electrical modulation at room temperature of magnetic properties in an extrinsic multiferroic fabricated by sputtering polycrystalline  $\text{Fe}_{81}\text{Ga}_{19}$  thin films onto (011)-cut and poled PMN-PZT ferroelectric single crystals.

In-plane azimuthal magnetization reversal measurements enabled to assess, under an applied electric field, the modification of the magnetic anisotropy character: the cubic component in thinner films (5 nm) shifts towards a predominant uniaxial component. This shift is accompanied by a  $90^\circ$  rotation of the as-deposited preferential anisotropy axis, and a relative remanent magnetization change of about 80%. In thicker films (60 nm), the random anisotropy character vanishes under  $E$  leaving out a coexisting cubic and uniaxial character.

With the assistance of small magnetic fields near  $\mu_0 H_c$  values, an electric field is capable of switching the magnetization state, and achieve a converse magnetoelectric coupling coefficient  $\alpha_{\text{CME}} = 2.7 \times 10^{-6} \text{ s.m}^{-1}$  at a given angle  $\varphi = 30^\circ$  between  $\mu_0 H$  and the deposition field direction  $\mu_0 H_{\text{dep}}$ . This sizable ME coupling is attributed to many important factors: the high in-plane piezoelectric coefficients of (011)-PMN-PZT, the reasonable magnetic properties of FeGa such as the high saturation magnetization and the high magnetoelastic coefficients, as well as the angular dependency of FeGa magnetic properties. This reported value of  $\alpha_{\text{CME}}$  is among the highest previously reported values in single-phase multiferroics or similar composites. We have also shed light for the first time on an azimuthal behavior of the  $\alpha_{\text{CME}}$  driven by, not only the anisotropic ferroelectric substrate, but

also the anisotropic FeGa.

This ME multiferroic composite promises good results regarding the self-bias effect in a dynamic measurement to achieve remanent CME, at zero magnetic bias field. Such highly performant combined materials may increase the pace towards novel multifunctional devices such as microwave devices, where anisotropy is required, and electrically tunable magnetoelectric memories.

We also find that the FeGa anisotropy characters manifest the same at room temperature on two different types of substrates, i.e. amorphous glass and single-crystalline ferroelectric PMN-PZT. However at low temperatures the mechanical nature of the substrate strongly influences

the magnetic behavior. This provides a useful insight into the bonding nature of magnetostrictive and piezoelectric materials, and ultimately into the performance of CME composites in complex environments involving cryogenic temperatures.

## ACKNOWLEDGMENTS

We wish to acknowledge the support of Region Bretagne (ARED), France, in co-funding the PhD of W.J. This work was also supported by South African National Research Foundation (Grant No 80880) and the URC and FRC of the University of Johannesburg, South Africa.

- 
- [1] N. A. Spaldin and M. Fiebig, The renaissance of magnetoelectric multiferroics, *Science* **309**, 391 (2005).
  - [2] S. Fusil, V. Garcia, A. Barthélemy, and M. Bibes, Magnetoelectric devices for spintronics, *Annual Review of Materials Research* **44**, 91 (2014), <https://doi.org/10.1146/annurev-matsci-070813-113315>.
  - [3] W. Eerenstein, N. D. Mathur, and J. F. Scott, Multiferroic and magnetoelectric materials, *Nature* **442**, 759 (2006).
  - [4] F. Matsukura, Y. Tokura, and H. Ohno, Control of magnetism by electric fields, *Nature Nanotechnology* **10**, 209 (2015).
  - [5] J.-M. Hu, Z. Li, L.-Q. Chen, and C.-W. Nan, High-density magnetoresistive random access memory operating at ultralow voltage at room temperature, *Nature Communications* **2**, 10.1038/ncomms1564 (2011).
  - [6] D. Chiba, M. Sawicki, Y. Nishitani, Y. Nakatani, F. Matsukura, and H. Ohno, Magnetization vector manipulation by electric fields, *Nature* **455**, 515 (2008).
  - [7] J. T. Heron, M. Trassin, K. Ashraf, M. Gajek, Q. He, S. Y. Yang, D. E. Nikonov, Y.-H. Chu, S. Salahuddin, and R. Ramesh, Electric-Field-Induced Magnetization Reversal in a Ferromagnet-Multiferroic Heterostructure, *Phys. Rev. Lett.* **107** (2011).
  - [8] W. Eerenstein, M. Wiora, J. L. Prieto, J. F. Scott, and N. D. Mathur, Giant sharp and persistent converse magnetoelectric effects in multiferroic epitaxial heterostructures, *Nature Materials* **6**, 348 (2007).
  - [9] T. Zhao, A. Scholl, F. Zavaliche, K. Lee, M. Barry, A. Doran, M. P. Cruz, Y. H. Chu, C. Ederer, N. A. Spaldin, R. R. Das, D. M. Kim, S. H. Baek, C. B. Eom, and R. Ramesh, Electrical control of antiferromagnetic domains in multiferroic BiFeO<sub>3</sub> films at room temperature, *Nature Materials* **5**, 823 (2006).
  - [10] N. Hur, S. Park, P. A. Sharma, J. S. Ahn, S. Guha, and S.-W. Cheong, Electric polarization reversal and memory in a multiferroic material induced by magnetic fields, *Nature* **429**, 392 (2004).
  - [11] G. Catalan and J. F. Scott, Physics and applications of bismuth ferrite, *Advanced Materials* **21**, 2463 (2009).
  - [12] T. Hauguel, S. P. Pogossian, D. T. Dekadjevi, D. Spenato, J.-P. Jay, and J. Ben Youssef, Driving mechanism of exchange bias and magnetic anisotropy in multiferroic polycrystalline BiFeO<sub>3</sub>/permalloy bilayers, *Journal of Applied Physics* **112**, 093904 (2012).
  - [13] J. Richy, T. Hauguel, J.-P. Jay, S. P. Pogossian, B. Warot-Fonrose, C. J. Sheppard, J. L. Snyman, A. M. Strydom, J. B. Youssef, A. R. E. Prinsloo, D. Spenato, and D. T. Dekadjevi, Temperature dependence of exchange biased multiferroic BiFeO<sub>3</sub>/Ni<sub>81</sub>Fe<sub>19</sub> polycrystalline bilayer", *J. Phys. Appl. Phys.* **51**, 125308 (2018).
  - [14] W. Jahjah, J.-P. Jay, Y. Le Grand, A. Fessant, J. Richy, C. Marcelot, B. Warot-Fonrose, A. R. E. Prinsloo, C. J. Sheppard, D. T. Dekadjevi, and D. Spenato, Influence of mesoporous or parasitic BiFeO<sub>3</sub> structural state on the magnetization reversal in multiferroic BiFeO<sub>3</sub>/Ni<sub>81</sub>Fe<sub>19</sub> polycrystalline bilayers, *Journal of Applied Physics* **124**, 235309 (2018).
  - [15] H. Palneedi, V. Annapureddy, S. Priya, and J. Ryu, Status and Perspectives of Multiferroic Magnetoelectric Composite Materials and Applications, *Actuators* **5**, 9 (2016).
  - [16] Y. Wang, J. Hu, Y. Lin, and C.-W. Nan, Multiferroic magnetoelectric composite nanostructures, *NPG Asia Materials* **2**, 61 (2010).
  - [17] G. Srinivasan, Magnetoelectric Composites, *Annual Review of Materials Research* **40**, 153 (2010).
  - [18] C.-W. Nan, M. I. Bichurin, S. Dong, D. Viehland, and G. Srinivasan, Multiferroic magnetoelectric composites: Historical perspective, status, and future directions, *Journal of Applied Physics* **103**, 031101 (2008).
  - [19] C. A. F. Vaz, Electric field control of magnetism in multiferroic heterostructures, *Journal of Physics: Condensed Matter* **24**, 333201 (2012).
  - [20] T. Nan, Z. Zhou, M. Liu, X. Yang, Y. Gao, B. A. Assaf, H. Lin, S. Velu, X. Wang, H. Luo, J. Chen, S. Akhtar, E. Hu, R. Rajiv, K. Krishnan, S. Sreedhar, D. Heiman, B. M. Howe, G. J. Brown, and N. X. Sun, Quantification of strain and charge co-mediated magnetoelectric coupling on ultra-thin Permalloy/PMN-PT interface, *Scientific Reports* **4**, 3688 (2014).
  - [21] Z. Zhou, B. M. Howe, M. Liu, T. Nan, X. Chen, K. Mahalingam, N. X. Sun, and G. J. Brown, Interfacial charge-mediated non-volatile magnetoelectric coupling in Co<sub>0.3</sub>Fe<sub>0.7</sub>/Ba<sub>0.6</sub>Sr<sub>0.4</sub>TiO<sub>3</sub>/Nb:SrTiO<sub>3</sub> multiferroic heterostructures, *Scientific Reports* **5**, 7740 (2015).

- [22] V. Laukhin, V. Skumryev, X. Martí, D. Hrabovsky, F. Sánchez, M. V. García-Cuenca, C. Ferrater, M. Varela, U. Lüders, J. F. Bobo, and J. Fontcuberta, Electric-field control of exchange bias in multiferroic epitaxial heterostructures, *Phys. Rev. Lett.* **97**, 227201 (2006).
- [23] Y. Yang, Y. Gong, S. Ma, C. Shen, D. Wang, Q. Cao, Z. Zhong, and Y. Du, Electric-field control of exchange bias field in a Mn 50.1 Ni 39.3 Sn 10.6 /piezoelectric laminate, *Journal of Alloys and Compounds* **619**, 1 (2015).
- [24] M. Liu, J. Lou, S. Li, and N. X. Sun, E-Field Control of Exchange Bias and Deterministic Magnetization Switching in AFM/FM/FE Multiferroic Heterostructures, *Advanced Functional Materials* **21**, 2593 (2011).
- [25] C. Thiele, K. Dörr, O. Bilani, J. Rödel, and L. Schultz, Influence of strain on the magnetization and magnetoelectric effect in La 0.7 A 0.3 Mn O 3 / PMN - PT ( 001 ) ( A = Sr , Ca ), *Physical Review B* **75**, 10.1103/PhysRevB.75.054408 (2007).
- [26] J. J. Yang, Y. G. Zhao, H. F. Tian, L. B. Luo, H. Y. Zhang, Y. J. He, and H. S. Luo, Electric field manipulation of magnetization at room temperature in multiferroic CoFe<sub>2</sub>O<sub>4</sub>/Pb(Mg<sub>1/3</sub>Nb<sub>2/3</sub>)<sub>0.7</sub>Ti<sub>0.3</sub>O<sub>3</sub> heterostructures, *Applied Physics Letters* **94**, 212504 (2009).
- [27] A. Alberca, C. Munuera, J. Azpeitia, B. Kirby, N. M. Nemes, A. M. Perez-Muñoz, J. Tornos, F. J. Mompean, C. Leon, J. Santamaria, and M. Garcia-Hernandez, Phase separation enhanced magneto-electric coupling in La<sub>0.7</sub>Ca<sub>0.3</sub>MnO<sub>3</sub>/BaTiO<sub>3</sub> ultra-thin films, *Scientific Reports* **5**, 17926 (2015).
- [28] M. Staruch, D. B. Gopman, Y. L. Iunin, R. D. Shull, S. F. Cheng, K. Bussmann, and P. Finkel, Reversible strain control of magnetic anisotropy in magnetoelectric heterostructures at room temperature, *Scientific Reports* **6**, 10.1038/srep37429 (2016).
- [29] T. Wu, A. Bur, K. P. Mohanchandra, K. Wong, K. L. Wang, C. S. Lynch, and G. P. Carman, Giant electric-field-induced reversible and permanent magnetization reorientation on magnetoelectric Ni/(011) [Pb(Mg<sub>1/3</sub>Nb<sub>2/3</sub>)O<sub>3</sub>](1-x)-[PbTiO<sub>3</sub>]x heterostructure, *Applied Physics Letters* **98**, 012504 (2011).
- [30] S. Zhang, Y. Zhao, X. Xiao, Y. Wu, S. Rizwan, L. Yang, P. Li, J. Wang, M. Zhu, H. Zhang, X. Jin, and X. Han, Giant electrical modulation of magnetization in Co<sub>40</sub>Fe<sub>40</sub>B<sub>20</sub>/Pb(Mg<sub>1/3</sub>Nb<sub>2/3</sub>)<sub>0.7</sub>Ti<sub>0.3</sub>O<sub>3</sub>(011) heterostructure, *Scientific Reports* **4**, 10.1038/srep03727 (2015).
- [31] C. Yang, P. Li, Y. Wen, A. Yang, D. Wang, F. Zhang, and J. Zhang, Giant Converse Magnetoelectric Effect in PZT/FeCuNbSiB/FeGa/FeCuNbSiB/PZT Laminates Without Magnetic Bias Field, *IEEE Transactions on Magnetics* **51**, 1 (2015).
- [32] A. K. Biswas, H. Ahmad, J. Atulasimha, and S. Bandyopadhyay, Experimental Demonstration of Complete 180° Reversal of Magnetization in Isolated Co Nanomagnets on a PMN-PT Substrate with Voltage Generated Strain, *Nano letters* **17**, 3478 (2017).
- [33] Y. Cheng, B. Peng, Z. Hu, Z. Zhou, and M. Liu, Recent development and status of magnetoelectric materials and devices, *Physics Letters A* **382**, 3018 (2018).
- [34] E. Du Trémolet de Lacheisserie, *Magnetostriction: theory and applications of magnetoelasticity* (Boca Raton: CRC Press, 1993).
- [35] S. Zhang, S.-M. Lee, D.-H. Kim, H.-Y. Lee, and T. R. Shrout, Electromechanical properties of pmn-pzt piezoelectric single crystals near morphotropic phase boundary compositions, *Journal of the American Ceramic Society* **90**, 3859 (2007).
- [36] S. Zhang and T. R. Shrout, Relaxor-PT single crystals: Observations and developments, *IEEE transactions on ultrasonics, ferroelectrics, and frequency control* **57** (2010).
- [37] T. Richter, S. Denner, C. Schuh, E. Suvaci, and R. Moos, Textured PMN-PT and PMN-PZT, *Journal of the American Ceramic Society* **91**, 929 (2008).
- [38] IEEE Standard for Relaxor-Based Single Crystals for Transducer and Actuator Applications 10.1109/IEEESTD.2017.8241013.
- [39] H. Palneedi, S.-M. Na, G.-T. Hwang, M. Peddigari, K. W. Shin, K. H. Kim, and J. Ryu, Highly tunable magnetoelectric response in dimensional gradient laminate composites of Fe-Ga alloy and Pb(Mg<sub>1/3</sub>Nb<sub>2/3</sub>)O<sub>3</sub>-Pb(Zr,Ti)O<sub>3</sub> single crystal, *Journal of Alloys and Compounds* **765**, 764 (2018).
- [40] F. Wang, S. W. Or, X. Zhao, and H. Luo, Cryogenic dielectric and piezoelectric activities in rhombohedral (1 - x )Pb(Mg <sub>1/3</sub> Nb <sub>2/3</sub> )O <sub>3</sub> - x PbTiO <sub>3</sub> single crystals with different crystallographic orientations, *Journal of Physics D: Applied Physics* **42**, 182001 (2009).
- [41] G.-T. Hwang, H. Palneedi, B. M. Jung, S. J. Kwon, M. Peddigari, Y. Min, J.-W. Kim, C.-W. Ahn, J.-J. Choi, B.-D. Hahn, J.-H. Choi, W.-H. Yoon, D.-S. Park, S.-B. Lee, Y. Choe, K.-H. Kim, and J. Ryu, Enhancement of Magnetoelectric Conversion Achieved by Optimization of Interfacial Adhesion Layer in Laminate Composites, *ACS Applied Materials & Interfaces* **10**, 32323 (2018).
- [42] L. Luo, H. Wang, Y. Tang, X. Zhao, Z. Feng, D. Lin, and H. Luo, Ultrahigh transverse strain and piezoelectric behavior in (1-x)Pb(Mg<sub>1/3</sub>Nb<sub>2/3</sub>)O<sub>3</sub>-xPbTiO<sub>3</sub> crystals, *Journal of Applied Physics* **99**, 024104 (2006).
- [43] J. Luo and S. Zhang, Advances in the Growth and Characterization of Relaxor-PT-Based Ferroelectric Single Crystals, *Crystals* **4**, 306 (2014).
- [44] D. Rajaram Patil, R. C. Kambale, Y. Chai, W.-H. Yoon, D.-Y. Jeong, D.-S. Park, J.-W. Kim, J.-J. Choi, C.-W. Ahn, B.-D. Hahn, S. Zhang, K. Hoon Kim, and J. Ryu, Multiple broadband magnetoelectric response in thickness-controlled Ni/[011] Pb(Mg <sub>1/3</sub> Nb <sub>2/3</sub> )O <sub>3</sub> -Pb(Zr,Ti)O <sub>3</sub> single crystal/Ni laminates, *Applied Physics Letters* **103**, 052907 (2013).
- [45] R. C. Kambale, W.-H. Yoon, D.-S. Park, J.-J. Choi, C.-W. Ahn, J.-W. Kim, B.-D. Hahn, D.-Y. Jeong, B. Chul Lee, G.-S. Chung, and J. Ryu, Magnetoelectric properties and magnetomechanical energy harvesting from stray vibration and electromagnetic wave by Pb(Mg <sub>1/3</sub> Nb <sub>2/3</sub> )O <sub>3</sub> -Pb(Zr,Ti)O <sub>3</sub> single crystal/Ni cantilever, *Journal of Applied Physics* **113**, 204108 (2013).
- [46] J. Ryu, J.-E. Kang, Y. Zhou, S.-Y. Choi, W.-H. Yoon, D.-S. Park, J.-J. Choi, B.-D. Hahn, C.-W. Ahn, J.-W. Kim, Y.-D. Kim, S. Priya, S. Y. Lee, S. Jeong, and D.-Y. Jeong, Ubiquitous magneto-mechano-electric generator, *Energy & Environmental Science* **8**, 2402 (2015).
- [47] H. Palneedi, V. Annapureddy, H.-Y. Lee, J.-J. Choi, S.-Y. Choi, S.-Y. Chung, S.-J. L. Kang, and J. Ryu, Strong and anisotropic magnetoelectricity in composites

- of magnetostrictive Ni and solid-state grown lead-free piezoelectric BZT–BCT single crystals, *Journal of Asian Ceramic Societies* **5**, 36 (2017).
- [48] O. Bilgen, M. Amin Karami, D. J. Inman, and M. I. Friswell, The actuation characterization of cantilevered unimorph beams with single crystal piezoelectric materials, *Smart Materials and Structures* **20**, 055024 (2011).
- [49] J. Lian, F. Ponchel, N. Tiercelin, Y. Chen, D. Rémiens, T. Lasri, G. Wang, P. Pernod, W. Zhang, and X. Dong, Electric field tuning of magnetism in heterostructure of yttrium iron garnet film/lead magnesium niobate-lead zirconate titanate ceramic, *Applied Physics Letters* **112**, 162904 (2018).
- [50] C.-S. Park, K.-H. Cho, M. A. Arat, J. Evey, and S. Priya, High magnetic field sensitivity in  $\text{Pb}(\text{Zr,Ti})\text{O}_3\text{--Pb}(\text{Mg}_{1/3}\text{Nb}_{2/3})\text{O}_3$  single crystal/Terfenol-D/Metglas magnetoelectric laminate composites, *Journal of Applied Physics* **107**, 094109 (2010).
- [51] V. Annapureddy, S.-M. Na, G.-T. Hwang, M. G. Kang, R. Sriramdas, H. Palneedi, W.-H. Yoon, B.-D. Hahn, J.-W. Kim, C.-W. Ahn, D.-S. Park, J.-J. Choi, D.-Y. Jeong, A. B. Flatau, M. Peddigari, S. Priya, K.-H. Kim, and J. Ryu, Exceeding milli-watt powering magneto-mechano-electric generator for standalone-powered electronics, *Energy & Environmental Science* 10.1039/C7EE03429F (2018).
- [52] Z. Chu, V. Annapureddy, M. PourhosseiniAsl, H. Palneedi, J. Ryu, and S. Dong, Dual-stimulus magnetoelectric energy harvesting, *MRS Bulletin* **43**, 199 (2018).
- [53] A. E. Clark, J. B. Restorff, M. Wun-Fogle, T. A. Lograsso, and D. L. Schlager, Magnetostrictive properties of body-centered cubic fe-ga and fe-ga-al alloys, *IEEE Transactions on Magnetics* **36**, 3238 (2000).
- [54] J. Atulasimha and A. B. Flatau, A review of magnetostrictive iron–gallium alloys, *Smart Materials and Structures* **20**, 043001 (2011).
- [55] W. Jahjah, R. Manach, Y. L. Grand, A. Fessant, B. Warot-Fonrose, A. R. E. Prinsloo, C. J. Sheppard, D. T. Dekadjevi, D. Spenato, and J.-P. Jay, Thickness dependence of magnetization reversal and magnetostriction in FeGa thin films, arXiv:1903.05397 [cond-mat] (2019).
- [56] P. Finkel, R. Pérez Moyet, M. Wun-Fogle, J. Restorff, J. Kosior, M. Staruch, J. Stace, and A. Amin, Non-Resonant Magnetoelectric Energy Harvesting Utilizing Phase Transformation in Relaxor Ferroelectric Single Crystals, *Actuators* **5**, 2 (2015).
- [57] L. Wang, Z. Du, C. Fan, L. Xu, H. Zhang, and D. Zhao, Magnetoelectric properties of Fe–Ga/BaTiO<sub>3</sub> laminate composites, *Journal of Alloys and Compounds* **509**, 508 (2011).
- [58] S. Dong, J. Zhai, N. Wang, F. Bai, J. Li, D. Viehland, and T. A. Lograsso, Fe–Ga/Pb(Mg<sub>1/3</sub>Nb<sub>2/3</sub>)O<sub>3</sub>–PbTiO<sub>3</sub> magnetoelectric laminate composites, *Applied Physics Letters* **87**, 222504 (2005).
- [59] D. E. Parkes, S. A. Cavill, A. T. Hindmarch, P. Wadley, F. McGee, C. R. Staddon, K. W. Edmonds, R. P. Campion, B. L. Gallagher, and A. W. Rushforth, Non-volatile voltage control of magnetization and magnetic domain walls in magnetostrictive epitaxial thin films, *Applied Physics Letters* **101**, 072402 (2012).
- [60] Y. Xie, Q. Zhan, Y. Liu, G. Dai, H. Yang, Z. Zuo, B. Chen, B. Wang, Y. Zhang, X. Rong, and R.-W. Li, Electric-field control of magnetic anisotropy in  $\text{Fe}_{81}\text{Ga}_{19}/\text{BaTiO}_3$  heterostructure films, *AIP Advances* **4**, 117113 (2014).
- [61] M. Liu and N. X. Sun, Voltage control of magnetism in multiferroic heterostructures, *Philosophical Transactions of the Royal Society A: Mathematical, Physical and Engineering Sciences* **372**, 20120439 (2014).
- [62] H. Ahmad, J. Atulasimha, and S. Bandyopadhyay, Electric field control of magnetic states in isolated and dipole-coupled FeGa nanomagnets delineated on a PMN-PT substrate, *Nanotechnology* **26**, 401001 (2015).
- [63] N. N. Phuoc and C. K. Ong, Electrical manipulation of electromagnetic properties of  $\text{FeGa}/[\text{Pb}(\text{Mg}_{1/3}\text{Nb}_{2/3})\text{O}_3]_{0.68}\text{--}[\text{PbTiO}_3]_{0.32}$  multiferroic heterostructures, *Journal of Materials Science: Materials in Electronics* **28**, 5628 (2017).
- [64] Y. Zhang, C. Huang, M. Turghun, Z. Duan, F. Wang, and W. Shi, Electric-regulated enhanced in-plane uniaxial anisotropy in FeGa/PMN–PT composite using oblique pulsed laser deposition, *Applied Physics A* **124**, 10.1007/s00339-018-1723-1 (2018).
- [65] Z. Hu, T. Nan, X. Wang, M. Staruch, Y. Gao, P. Finkel, and N. X. Sun, Voltage control of magnetism in FeGaB/PIN-PMN-PT multiferroic heterostructures for high-power and high-temperature applications, *Applied Physics Letters* **106**, 022901 (2015).
- [66] J. Lou, M. Liu, D. Reed, Y. Ren, and N. X. Sun, Giant Electric Field Tuning of Magnetism in Novel Multiferroic FeGaB/Lead Zinc Niobate-Lead Titanate (PZN-PT) Heterostructures, *Advanced Materials* **21**, 4711 (2009).
- [67] J. Zhang, P. Li, Y. Wen, W. He, A. Yang, D. Wang, C. Yang, and C. Lu, Giant self-biased converse magnetoelectric effect in multiferroic heterostructure with single-phase magnetostrictive materials, *Appl. Phys. Lett.* **105**, 172408 (2014).
- [68] S. Chul Yang, K.-H. Cho, C.-S. Park, and S. Priya, Self-biased converse magnetoelectric effect, *Appl. Phys. Lett.* **99**, 202904 (2011).
- [69] T. Fitchorov, Y. Chen, L. Jiang, G. Zhang, Z. Zhao, C. Vittoria, and V. G. Harris, Converse Magnetoelectric Effect in a Fe-Ga/PMN-PT Laminated Multiferroic Heterostructure for Field Generator Applications, *IEEE Transactions on Magnetics* **47**, 4050 (2011).
- [70] S. K. Mandal, G. Sreenivasulu, V. M. Petrov, and G. Srinivasan, Magnetization-graded multiferroic composite and magnetoelectric effects at zero bias, *Phys. Rev. B* **84**, 014432 (2011).
- [71] Y. Zhou, D. Maurya, Y. Yan, G. Srinivasan, E. Quandt, and S. Priya, Self-Biased Magnetoelectric Composites: An Overview and Future Perspectives, *Energy Harvesting and Systems* **3**, 1 (2016).
- [72] M. Fiebig, T. Lottermoser, D. Meier, and M. Trassin, The evolution of multiferroics, *Nature Reviews Materials* **1**, 16046 (2016).
- [73] Ceracomp Co. Ltd., Korea, <http://www.ceracomp.com>.
- [74] M. Shanthi, L. C. Lim, K. K. Rajan, and J. Jin, Complete sets of elastic, dielectric, and piezoelectric properties of flux-grown [011]-poled  $\text{Pb}(\text{Mg}_{1/3}\text{Nb}_{2/3})\text{O}_3$ –(28–32)%  $\text{PbTiO}_3$  single crystals, *Applied Physics Letters* **92**, 142906 (2008).
- [75] Schott D 263 TM Glass, [https://www.schott.com/nexterion/english/products/uncoated-substrates/d263.html?highlighted\\_text=d263](https://www.schott.com/nexterion/english/products/uncoated-substrates/d263.html?highlighted_text=d263).

- [76] Evico Magnetics, Dresden, <http://www.evico-magnetics.de>.
- [77] Cryogenic Ltd., London, UK, Cryogen free magnet system user manual (2016).
- [78] P. Zhao, M. Bao, A. Bur, J. L. Hockel, K. Wong, K. P. Mohanchandra, C. S. Lynch, and G. P. Carman, Domain engineered switchable strain states in ferroelectric (011)  $[\text{Pb}(\text{Mg}_{1/3}\text{Nb}_{2/3})\text{O}_3]_{(1-x)}-[\text{PbTiO}_3]_x$  (PMN-PT,  $x \approx 0.32$ ) single crystals, *Journal of Applied Physics* **109**, 124101 (2011).
- [79] W. Huang, S. Yang, and X. Li, Multiferroic heterostructures and tunneling junctions, *Journal of Materiomics* **1**, 263 (2015).
- [80] S. Zhang, Y. G. Zhao, P. S. Li, J. J. Yang, S. Rizwan, J. X. Zhang, J. Seidel, T. L. Qu, Y. J. Yang, Z. L. Luo, Q. He, T. Zou, Q. P. Chen, J. W. Wang, L. F. Yang, Y. Sun, Y. Z. Wu, X. Xiao, X. F. Jin, J. Huang, C. Gao, X. F. Han, and R. Ramesh, Electric-Field Control of Nonvolatile Magnetization in  $\text{Co}_{40}\text{Fe}_{40}\text{B}_{20}/\text{Pb}(\text{Mg}_{1/3}\text{Nb}_{2/3})_{0.7}\text{Ti}_{0.3}\text{O}_3$  Structure at Room Temperature, *Physical Review Letters* **108**, 10.1103/PhysRevLett.108.137203 (2012).
- [81] L. Yang, Y. Zhao, S. Zhang, P. Li, Y. Gao, Y. Yang, H. Huang, P. Miao, Y. Liu, A. Chen, C. W. Nan, and C. Gao, Bipolar loop-like non-volatile strain in the (001)-oriented  $\text{Pb}(\text{Mg}_{1/3}\text{Nb}_{2/3})\text{O}_3$ - $\text{PbTiO}_3$  single crystals, *Scientific Reports* **4**, 4591 (2015).
- [82] Y. Wei, C. Gao, Z. Chen, S. Xi, W. Shao, P. Zhang, G. Chen, and J. Li, Four-state memory based on a giant and non-volatile converse magnetoelectric effect in  $\text{FeAl}/\text{PIN-PMN-PT}$  structure, *Scientific Reports* **6**, 10.1038/srep30002 (2016).
- [83] J. Wang, D. Pesquera, R. Mansell, S. van Dijken, R. P. Cowburn, M. Ghidini, and N. D. Mathur, Giant non-volatile magnetoelectric effects via growth anisotropy in  $\text{Co}_{40}\text{Fe}_{40}\text{B}_{20}$  films on PMN-PT substrates, *Appl. Phys. Lett.* **114**, 092401 (2019).
- [84] C. Jiang, C. Zhang, C. Dong, D. Guo, and D. Xue, Electric field tuning of non-volatile three-state magnetoelectric memory in  $\text{FeCo-NiFe}_2\text{O}_4/\text{Pb}(\text{Mg}_{1/3}\text{Nb}_{2/3})_{0.7}\text{Ti}_{0.3}\text{O}_3$  heterostructures, *Applied Physics Letters* **106**, 122406 (2015).
- [85] D. Damjanovic, Hysteresis in Piezoelectric and Ferroelectric Materials, in *The Science of Hysteresis* (Elsevier, 2006) pp. 337–465.
- [86] X. Guo, X. Han, Y. Zuo, J. Zhang, D. Li, B. Cui, K. Wu, J. Yun, T. Wang, Y. Peng, and L. Xi, Electric field induced magnetic anisotropy transition from fourfold to twofold symmetry in (001)  $0.68\text{Pb}(\text{Mg}_{1/3}\text{Nb}_{2/3})\text{O}_3-0.32\text{PbTiO}_3/\text{Fe}_{0.86}\text{Si}_{0.14}$  epitaxial heterostructures, *Applied Physics Letters* **108**, 152401 (2016).
- [87] Y. Chen, A. L. Geiler, T. Fitchorov, C. Vittoria, and V. G. Harris, Time domain analyses of the converse magnetoelectric effect in a multiferroic metallic glass-relaxor ferroelectric heterostructure, *Applied Physics Letters* **95**, 182501 (2009).
- [88] D. C. Lupascu and C. Verdier, Fatigue anisotropy in lead-zirconate-titanate, *Journal of the European Ceramic Society* **24**, 1663 (2004), electroceramics VIII.
- [89] V. Gopalan and M. C. Gupta, Observation of internal field in  $\text{LiTaO}_3$  single crystals: Its origin and time-temperature dependence, *Applied Physics Letters* **68**, 888 (1996).
- [90] Y. Noguchi, I. Miwa, Y. Goshima, and M. Miyayama, Defect Control for Large Remanent Polarization in Bismuth Titanate Ferroelectrics – Doping Effect of Higher-Valent Cations –, *Japanese Journal of Applied Physics* **39**, L1259 (2000).
- [91] J. Cullen, P. Zhao, and M. Wuttig, Anisotropy of crystalline ferromagnets with defects, *Journal of Applied Physics* **101**, 123922 (2007).
- [92] A. Begué, M. G. Proietti, J. I. Arnaud, and M. Ciria, Magnetic ripple domain structure in  $\text{FeGa}/\text{MgO}$  thin films, *arXiv:1905.09180 [cond-mat]* (2019), *arXiv:1905.09180 [cond-mat]*.
- [93] R. O. Cherifi, V. Ivanovskaya, L. C. Phillips, A. Zobel, I. C. Infante, E. Jacquet, V. Garcia, S. Fusil, P. R. Bridon, N. Guiblin, A. Mougin, A. A. Ünal, F. Kronast, S. Valencia, B. Dkhil, A. Barthélémy, and M. Bibes, Electric-field control of magnetic order above room temperature, *Nature Materials* **13**, 345 (2014).
- [94] J. T. Heron, J. L. Bosse, Q. He, Y. Gao, M. Trassin, L. Ye, J. D. Clarkson, C. Wang, J. Liu, S. Salahuddin, D. C. Ralph, D. G. Schlom, J. Iñiguez, B. D. Huey, and R. Ramesh, Deterministic switching of ferromagnetism at room temperature using an electric field, *Nature* **516**, 370 (2014).
- [95] G. Wu, R. Zhang, and N. Zhang, Enhanced converse magnetoelectric effect in cylindrical piezoelectric-magnetostrictive composites, *The European Physical Journal Applied Physics* **76**, 10602 (2016).
- [96] J. Han, J. Zhang, and Y. Gao, A nonlinear magneto-mechanical-thermal-electric coupling model of Terfenol-D/PZT/Terfenol-D and Ni/PZT/Ni laminates, **466**, 200 (2018).
- [97] D. A. Burdin, Y. K. Fetisov, D. V. Chashin, and N. A. Ekonomov, Temperature dependence of the characteristics of the resonant magnetoelectric effect in a lead magnesium niobate-lead titanate/nickel structure, *Tech. Phys. Lett.* **38**, 661 (2012).
- [98] Y. Zhang, Q. Zhan, X. Rong, H. Li, Z. Zuo, Y. Liu, B. Wang, and R.-W. Li, Influence of Thermal Deformation on Exchange Bias in  $\text{FeGa}/\text{IrMn}$  Bilayers Grown on Flexible Polyvinylidene Fluoride Membranes, *IEEE Transactions on Magnetics* **52**, 1 (2016).
- [99] Y. Liu, B. Wang, Q. Zhan, Z. Tang, H. Yang, G. Liu, Z. Zuo, X. Zhang, Y. Xie, X. Zhu, B. Chen, J. Wang, and R.-W. Li, Positive temperature coefficient of magnetic anisotropy in polyvinylidene fluoride (PVDF)-based magnetic composites, *Sci Rep* **4**, 6615 (2015).
- [100] Y. Liu, Q. Zhan, G. Dai, X. Zhang, B. Wang, G. Liu, Z. Zuo, X. Rong, H. Yang, X. Zhu, Y. Xie, B. Chen, and R.-W. Li, Thermally assisted electric field control of magnetism in flexible multiferroic heterostructures, *Scientific Reports* **4**, 10.1038/srep06925 (2015).